This is a repository copy of *A framework for modelling whole-lung and regional TLCO using hyperpolarised 129Xe lung MRI*.

White Rose Research Online URL for this paper:
https://eprints.whiterose.ac.uk/218257/

Version: Published Version

A framework for modelling whole-lung and regional transfer factor of the lung for carbon monoxide using hyperpolarised xenon-129 lung magnetic resonance imaging

Jemima H. Pilgrim-Morris [1], Laurie J. Smith [1], Helen Marshall [1,2], Bilal A. Tahir[1,2], Guilhem J. Collier[1,2], Neil J. Stewart [1,2] and Jim M. Wild[1,2]

[1]POLARIS, Section of Medical Imaging and Technologies, Division of Clinical Medicine, School of Medicine and Population Health, University of Sheffield, Sheffield, UK. [2]Insigneo Institute for In Silico Medicine, University of Sheffield, Sheffield, UK.

Corresponding author: Jim M. Wild (j.m.wild@sheffield.ac.uk)

Abstract

Background Pulmonary gas exchange is assessed by the transfer factor of the lungs (T_L) for carbon monoxide (T_{LCO}), and can also be measured with inhaled xenon-129 (^{129}Xe) magnetic resonance imaging (MRI). A model has been proposed to estimate T_L from ^{129}Xe MRI metrics, but this approach has not been fully validated and does not utilise the spatial information provided by three-dimensional ^{129}Xe MRI.

Methods Three models for predicting T_L from ^{129}Xe MRI metrics were compared: 1) a previously-published physiology-based model, 2) multivariable linear regression and 3) random forest regression. Models were trained on data from 150 patients with asthma and/or COPD. The random forest model was applied voxel-wise to ^{129}Xe images to yield regional T_L maps.

Results Coefficients of the physiological model were found to differ from previously reported values. All models had good prediction accuracy with small mean absolute error (MAE): 1) 1.24± 0.15 mmol·min^{-1}·kPa^{-1}, 2) 1.01±0.06 mmol·min^{-1}·kPa^{-1}, 3) 0.995±0.129 mmol·min^{-1}·kPa^{-1}. The random forest model performed well when applied to a validation group of post-COVID-19 patients and healthy volunteers (MAE=0.840 mmol·min^{-1}·kPa^{-1}), suggesting good generalisability. The feasibility of producing regional maps of predicted T_L was demonstrated and the whole-lung sum of the T_L maps agreed with measured T_{LCO} (MAE=1.18 mmol·min^{-1}·kPa^{-1}).

Conclusion The best prediction of T_{LCO} from ^{129}Xe MRI metrics was with a random forest regression framework. Applying this model on a voxel-wise level to create parametric T_L maps provides a useful tool for regional visualisation and clinical interpretation of ^{129}Xe gas exchange MRI.

Introduction

Pulmonary gas exchange function is usually evaluated using the carbon monoxide (CO) transfer factor (T_{LCO}) pulmonary function test (PFT), in which the patient inhales a test gas containing 0.3% CO and 0.3% tracer gas, such as helium, and holds their breath at total lung capacity (TLC) for 10 s [1]. The dilution of the tracer gas is used to calculate the number of accessible alveolar units (V_A) and the rate of disappearance of CO from the alveolar gas gives the gas exchange efficiency per unit (K_{CO}). Together, these measurements yield T_{LCO}, which represents the whole-lung average efficiency of gas transfer from the alveoli to the bloodstream. Although widely used [2], T_{LCO} measurement is a breathing test, measured at the mouth, and therefore lacks regional gas exchange information.

An alternative method to quantify pulmonary gas transfer is lung magnetic resonance imaging (MRI) with inhaled hyperpolarised ^{129}Xe gas. ^{129}Xe MRI is commonly used to image lung ventilation, where the

presence of airway obstruction leads to poor/no ventilation in the form of low/no signal on images [3, 4]. In addition, due to its solubility in the alveolar parenchymal tissue, capillary blood plasma and red blood cells (RBCs), ^{129}Xe MRI can quantitatively measure regional gas exchange limitation. ^{129}Xe exhibits distinct magnetic resonance signals when present in the alveoli, when dissolved in the lung tissue and plasma (collectively referred to as "membrane" (M)) and when in the RBCs [5]. Several methods have been designed to simultaneously image xenon in each of these three environments [5–9]. The ratios of the respective signals (RBC:M, RBC:gas and M:gas) are used to quantify gas transfer and are sensitive to gas exchange limitation in COPD [10–12], interstitial lung disease [7, 13, 14] and post-COVID-19 lung disease [15–17]. However, these gas exchange ratios lack a well-defined conventional physiological interpretation, which may hinder their clinical translation.

There are parallels between the measurements made with ^{129}Xe MRI and the constituent components of T_{LCO} (see Theory below), illustrated in figure 1. A model has been proposed by WANG et al. [18] to exploit these similarities by using features derived from ^{129}Xe ventilation and gas exchange imaging, along with V_A and K_{CO} from PFT, to predict T_{LCO}. However, the generalisability of this model is not clear, because the same data were used to both train the model and test its performance, leading to potentially biased results. Most commonly used T_{LCO} prediction models are based on participant demographics such as age and sex [19–22]. Indeed, the model-based prediction of T_{LCO} from ^{129}Xe MRI metrics may be improved by considering age and sex, as both affect ^{129}Xe MRI gas exchange metrics [23–25]. Furthermore, previous work [18] used the whole-lung average metrics from ^{129}Xe imaging to predict whole-lung T_{LCO}, which does not utilise the regional information offered by imaging. Here we propose that inputting the imaging maps to the predictive models instead would allow for regional visualisation of T_{LCO}.

The objectives of this work were therefore to 1) evaluate the model of WANG et al. [18] in a large cohort of asthma and COPD patients with a rigorous testing and training group validation strategy, and 2) build upon this model to predict both whole-lung and regional T_{LCO} using ^{129}Xe imaging and participant demographic data.
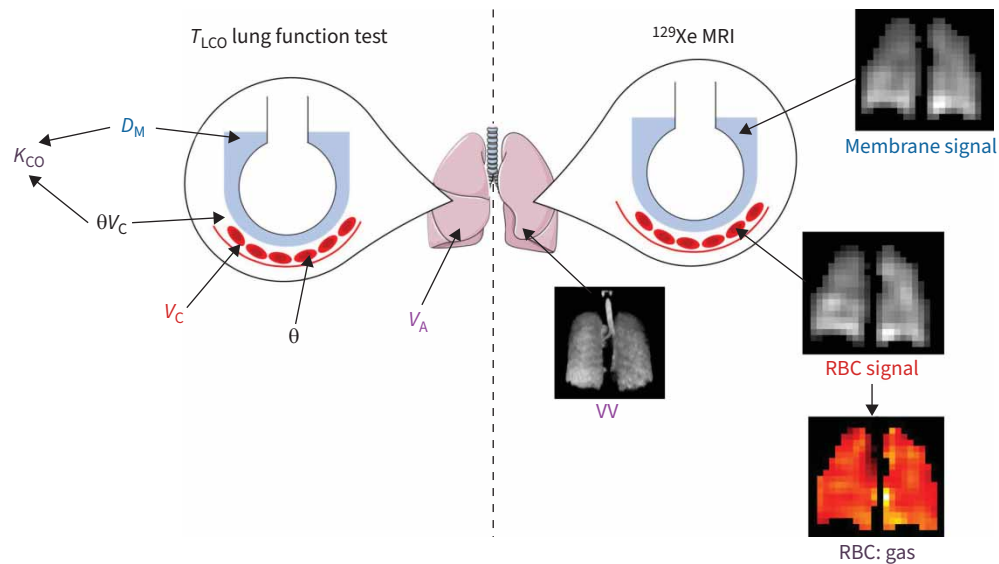
FIGURE 1 Schematic of the parallels between the underlying physiology measured by the transfer factor of the lung for carbon monoxide (T_{LCO}) lung function test and xenon-129 (^{129}Xe) magnetic resonance imaging (MRI). Like the membrane conductance (D_M), the ^{129}Xe membrane signal is dependent on the surface area and thickness of the alveolar membrane. The ^{129}Xe red blood cell (RBC) signal is influenced by both the gas exchange across the alveolar membrane and the capillary perfusion, so can be linked to the capillary blood volume (V_C). RBC:gas measures the transfer of gas from the alveolus, across the alveolar membrane and into the RBCs, so is analogous to the transfer coefficient (K_{CO}). VV is the volume of the lung where ^{129}Xe signal is detected, which is alike to the alveolar volume (V_A). θ is the reaction rate of CO with the RBCs. This figure was partly generated using Servier Medical Art, provided by Servier, licensed under a Creative Commons Attribution 3.0 unported license.

Theory

T_{LCO} represents the overall conductance of CO from the alveolar gas to the pulmonary capillary blood and is made up of two components:

$$\frac{1}{T_{\mathrm{LCO}}} = \frac{1}{D_{\mathrm{M}}} + \frac{1}{\theta V_{\mathrm{C}}}$$ (1)

where D_{M} is the membrane conductance and θV_{C} is the capillary blood conductance: θ is the reaction rate of CO with the RBCs and V_{C} is the capillary blood volume [26]. T_{LCO} also depends on the volume of the alveoli available for gas exchange, V_{A}:

$$T_{\mathrm{LCO}} = K_{\mathrm{CO}} V_{\mathrm{A}}$$ (2)

where K_{CO} is the transfer coefficient [1].

The model of WANG *et al.* [18] uses the following linear regression equations to predict whole-lung T_{LCO}, where k_{V}, k_{M} and k_{R} are coefficients found by fitting the model to measured data:

$$V_{\mathrm{A}} = k_{\mathrm{V}} \mathrm{VV}$$ (3)

$$D_{\mathrm{M}} = k_{\mathrm{M}} \mathrm{M:gas_{rel}} V_{\mathrm{A}}$$ (4)

$$\theta V_{\mathrm{C}} = k_{\mathrm{R}} \mathrm{RBC:gas_{rel}} V_{\mathrm{A}}$$ (5)

^{129}Xe MRI metrics: VV is the lung ventilated volume from ventilation imaging [27] and M:gas$_{\mathrm{rel}}$ and RBC:gas$_{\mathrm{rel}}$ are the dissolved ^{129}Xe signal ratio values divided by a healthy reference value. Equations 4 and 5 are then substituted into equation 1:

$$\frac{1}{K} = \frac{1}{k_{\mathrm{M}} \mathrm{M:gas_{rel}}} + \frac{1}{k_{\mathrm{R}} \mathrm{RBC:gas_{rel}}}$$ (6)

Here, the "CO" has been dropped from K_{CO} to specify that this is the predicted value from ^{129}Xe MRI metrics. The predicted K and V_{A} values are then multiplied to give the predicted transfer factor, T_{L}.

Materials and methods

Study participants

Models were trained on data from the Advanced Diagnostic Profiling (ADPro) substudy of the NOVEL observation longiTudinal studY (NOVELTY; ClinicalTrials.gov identifier: NCT02760329) of patients with asthma and/or COPD [28, 29]. Patients were recruited from primary care and had a mix of physician-assigned disease severity (mild, moderate or severe). The study involved two visits, at which participants underwent PFTs and MRI, with the second visit 12±2 months after the first. At visit one, ^{129}Xe ventilation and gas exchange imaging and PFTs were performed post-bronchodilator, whereas at visit two, ^{129}Xe imaging and PFTs were carried out both pre- and post-bronchodilator. Models were trained using the visit one dataset (n=165). Participants who had missing PFT or imaging data (due to missed appointments or scanner failure) were excluded and so the final training group consisted of 150 participants (table 1). 123 of 150 participants had pre-bronchodilator and 127 of 150 participants had post-bronchodilator ^{129}Xe imaging and PFT data at visit two.

Model validation was carried out on a separate cohort of 42 participants. 19 of 42 participants were part of the healthy control group of the Hyperpolarised Xenon Magnetic Resonance PuLmonary Imaging in PAtIeNts with Long-COVID (EXPLAIN) study [30]. The remaining 23 participants had been hospitalised due to COVID-19 (the MURCO: MUlti-nuclear MRI in COVID-19 study [17]) and their PFT and ^{129}Xe MRI data were from 1–12 months after hospital admission (median 6 months). The ADPro, EXPLAIN and MURCO studies were approved by the National Research Ethics Committee (REC reference numbers 16/EM/0439, 21/SC/0398 and 9/LO/1115).

MRI acquisition and pulmonary function testing

Imaging was performed on a 1.5T GE HDx whole-body clinical scanner, using hyperpolarised ^{129}Xe gas generated with a spin exchange optical pumping polariser [31]. ^{129}Xe ventilation imaging was acquired at end-inspiratory tidal volume with a maximum dose of 0.5 L ^{129}Xe and 0.5 L nitrogen (volume adjusted according to height; see supplementary table 1), using a three-dimensional (3D) steady-state free precession sequence and co-registered ^{1}H anatomical imaging [32]. A multi-echo time 3D radial spectroscopic sequence

TABLE 1 Patient demographics for the testing and validation groups

	All asthma and COPD	Asthma	COPD	Asthma + COPD	Post-COVID-19 hospitalisation	Healthy
Subjects (females), n	150 (75)	76 (39)	24 (17)	50 (19)	23 (3)	19 (13)
Age, years	60.6 (21.4–82.2)	54.2±13.8	66.5±8.4	63.6±10.5	62 (42–79)	40.9±9.5
Weight, kg	80.7±17.4	83.7±17.0	68.4±13.5	82.0±17.5	97.0±16.0	76.8±14.5
Height, cm	168.5±10.4	169.0±9.8	162.0±10.4	170.8±10.3	173.4±9.1	170.5±11.3
FEV_1, z-score	−0.65 (−4.49–2.66)	−0.10 (−3.84–2.66)	−1.89±1.60	−1.17±1.16	−0.70±1.00	0.13±0.75
T_{LCO}, mmol·min^{-1}·kPa^{-1}	7.56±2.55	8.48±2.18	5.16±2.46	7.01 (3.61–13.86)	6.00±1.68	8.84±2.19
T_{LCO}, z-score	−0.07 (−6.37–3.83)	0.29±1.14	−2.01±2.28	−0.65±1.30	−2.04±1.37	0.33±0.84
K_{CO}, mmol·min^{-1}·kPa^{-1}·L^{-1}	1.38±0.32	1.53±0.24	1.10±0.35	1.27±0.28	1.30±0.17	1.52±0.16
K_{CO}, z-score	−0.22 (−4.83–3.00)	0.30±1.07	−1.63±1.86	−0.67±1.29	−0.52±0.78	0.09±0.68
V_A, L	5.45±1.27	5.55±1.16	3.99 (2.76–7.81)	5.72±1.22	4.58±0.87	5.82±1.33
VV, L	4.47±0.86	4.46 (2.08–7.28)	4.03±0.74	4.60 (2.96–7.18)	3.80±0.43	4.39±0.74
M:gas	0.0091 (0.0051–0.0157)	0.0099±0.0021	0.0076±0.0017	0.0090±0.0024	0.0113 (0.0089–0.0125)	0.0087±0.0012
RBC:gas	0.0028 (0.0012–0.0068)	0.0031 (0.0017–0.0068)	0.0017 (0.0012–0.0034)	0.0025 (0.0013–0.0058)	0.0021 (0.0013–0.0039)	0.0032±0.0006

Normally distributed variables (determined using Shapiro–Wilk tests) are presented as mean±SD, whereas non-normally distributed variables are presented as median (minimum–maximum). FEV_1: forced expiratory volume in 1 s; T_{LCO}: transfer factor of the lungs for carbon monoxide; K_{CO}: transfer coefficient; V_A: alveolar volume; VV: ventilated volume; M:gas: membrane to gas signal ratio; RBC:gas: red blood cell to gas signal ratio.

[7] was used for dissolved ^{129}Xe imaging, performed in the same manner with a maximum dose of 1 L ^{129}Xe. For the training data, a flip angle of 40° and a repetition time of 40 ms were used for dissolved-phase imaging, whereas 22° and 15 ms were used for the validation group. More details on the differences between the two sequences are provided in the supplementary material. Additional anatomical imaging was performed using an ultrashort echo time sequence [33]. Measurement of T_{LCO}, K_{CO} and V_A were performed using a Vyaire PFT Pro (Vyaire Medical, Inc., Basingstoke, UK) and in accordance with international guidelines [34].

T$_{LCO}$ prediction models

Three T_L prediction models were evaluated:

1) Physiology-based linear regression: equations 3 and 6 were fitted on the training data, first using the values of k_V, k_M and k_R from [18] (model 1a) and separately using values found from a least squares solver to minimise the mean squared error (MSE) and best fit our training data (model 1b) in MATLAB (version R2022a, MathWorks, Natick, MA, USA). As in [18], RBC:gas and M:gas were normalised by healthy reference values, which were taken from a previous study [7].
2) Multivariable linear regression: features were chosen by first identifying correlated variables with a correlation matrix of possibilities (VV, M:gas, RBC:gas, age, sex, height and weight). Strongly correlated variables were removed, to avoid multi-collinearity. Separate prediction equations were then formed for K_{CO} and V_A by testing the predictive power of linear combinations of the remaining variables. Model fitting was performed with a linear regression solver from the scikit-learn Python toolbox (Python 3.9.12) [35].
3) Random forest regression: this is an ensemble machine-learning algorithm which combines predictions from many uncorrelated decision trees to output a prediction or classification [36]. Two regression models were trained using scikit-learn [35], to predict K and V_A separately, using the features identified from linear regression modelling. Tree splitting was based on minimisation of the MSE and model hyperparameters (supplementary table 2) were tuned using a grid search.

For both models 2 and 3, RBC:gas and M:gas were not normalised by the healthy reference values.

Model training and validation

The three models were initially trained using five-fold cross-validation: the training data were split randomly into five folds of 30 participants (stratified such that each group contained approximately the same proportion of asthma, COPD and combined asthma and COPD patients), and the models were fitted on four of the folds, with the remaining fold used to test the fit performance. This was repeated five times so that each fold acted as the testing data once. The model with the lowest MSE across the cross-validation folds was chosen as the final model and this was subsequently retrained on the entire training data and evaluated by applying to the validation set and ADPro visit two data.

Regional T$_{LCO}$ mapping

To derive regional maps of T_{LCO}, the final trained K_{CO} and V_A models were applied to each voxel of the RBC:gas map and a "relative" ventilation map determined from the gas-phase images of the gas exchange acquisition (figure 2). The maps were masked by applying a noise threshold to the M signal images. Ventilation distribution maps were found using equation 7:

$$V_r = VV \frac{I_r N_{voxel}}{I_{total}},\qquad(7)$$

where V_r is the relative ventilation at position r = (x, y, z), I_r is the gas signal intensity at position r, N_{voxel} is the total number of ventilated voxels (*i.e.* voxels in the lung mask) and I_{total} is the total gas signal intensity. This intermediate step was required so that the input to the V_A model (V_r) had the same units and order of magnitude as the VV data that the model was trained on. So that the $V_{A,r}$ maps had a clearer physiological meaning (VV per voxel), the initial V_A model output was scaled by N_{voxel}. The whole-lung predictions can be recovered from the regional maps by summing the fractional T_L and V_A values (T_{Lr} and $V_{A,r}$) and averaging the rate K (K_r):

$$T_L = \sum_r T_{Lr}\qquad(8)$$

$$V_A = \sum_r V_{A,r}\qquad(9)$$

$$K = \overline{K_r}\qquad(10)$$
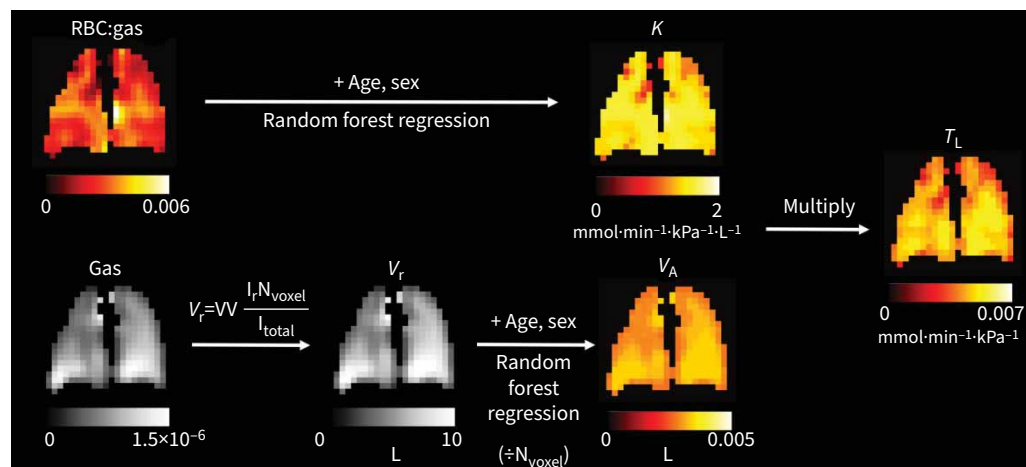
FIGURE 2 Regional random forest model: information on regional red blood cell (RBC) uptake and gas signal distribution from dissolved xenon-129 (^{129}Xe) imaging was utilised to produce regional maps of transfer factor (T_L). The transfer coefficient (K) prediction pipeline was applied to every voxel of the RBC:gas map, along with patient age and sex, to output a map of predicted K. For the prediction of accessible alveolar volume, an extra step (equation 7) was required to convert the gas signal map into a map of ventilation distribution (V_r), which had the required units of litres and order of magnitude. This involved finding the signal intensity of each pixel (I_r), dividing this by the mean signal intensity (I_{total}/N_{voxel}) and multiplying this fraction by the ventilated volume (VV) from ^{129}Xe ventilation imaging. The V_A random forest prediction was then applied to each voxel of this map, along with patient age and sex. The resulting map was renormalised by N_{voxel} so that it represented the ventilation per voxel and summed to give predicted V_A. This was then multiplied with the K map to obtain a map of T_L.

Statistical analysis

The predictive power of the models was assessed by calculating the MSE and R^2 of the linear fit of predicted and measured T_{LCO}, the mean absolute error (MAE) between the predicted and measured values and their Bland–Altman bias. Statistical analysis was carried out with RStudio (R version 4.3.0).

Results

Validation of physiological model

Model 1a: the model using linear regression coefficients from WANG *et al.* [18] (k_V=1.47, k_M=3.55 mmol·min^{-1}·kPa^{-1}·L^{-1} and k_R=4.55 mmol·min^{-1}·kPa^{-1}·L^{-1}) did not fit our training data well (table 2; MAE=2.66 mmol·min^{-1}·kPa^{-1}). Model 1b: the prediction accuracy was improved by refitting the values of k_V, k_M and k_R on our dataset (MAE=1.24±0.15 mmol·min^{-1}·kPa^{-1}); the refitted values were: k_V=1.21±0.01, k_M=4.51±0.26 mmol·min^{-1}·kPa^{-1}·L^{-1} and k_R=2.97±0.13 mmol·min^{-1}·kPa^{-1}·L^{-1}. Linear regression and Bland–Altman analysis of the measured and predicted T_{LCO} values are shown in supplementary figure 1.

Model	MSE (mmol^2·min^{-2}·kPa^{-2})	R^2	MAE (mmol·min^{-1}·kPa^{-1})	Bias (LOA) (mmol·min^{-1}·kPa^{-1})
1a	3.49	0.470	2.66	2.41 (−1.56–6.39)
1b	1.63±0.31	0.604±0.028	1.24±0.15	−0.14 (−3.25–2.97)
2	1.16±0.23	0.739±0.069	1.01±0.06	−0.02 (−2.55–2.52)
3	1.13±0.24	0.744±0.063	0.995±0.129	0.02 (−2.50–2.54)

TABLE 2 Evaluation of the four transfer factor prediction models on the training data

Model 1a: physiological model with coefficients from WANG *et al.* [18]; 1b: physiological model with refitted coefficients; 2: multivariable linear regression; 3: random forest regression. For models 1b, 2 and 3, the mean and SD across the five cross-validation folds is given. MSE: mean squared error; R^2: coefficient of determination; MAE: mean absolute error; LOA: limits of agreement.

Model development and validation

Model 2: M:gas and height were not included as features in the multivariable linear regression model because of their dependence on other variables. More information on the choice of model features is provided in the supplementary material. The final predictive equations were:

$$K = a_1 \frac{1}{\text{RBC}:\text{gas}} + a_2 \text{Age} + a_3 \text{Sex} + a_4 \tag{11}$$

and

$$V_A = b_1 \text{VV} + b_2 \text{Age} + b_3 \text{Sex} + b_4, \tag{12}$$

where sex is 0 for males and 1 for females. The fitted values of $a_{1,2,3,4}$ and $b_{1,2,3,4}$ can be found in supplementary table 3. Including participant age and sex as predictors improved the prediction of T_{LCO} compared with model 1b (MAE=1.01±0.06 mmol·min^{-1}·kPa^{-1}).

Model 3: the random forest regression model performed slightly better than linear regression (MAE=0.995± 0.129 mmol·min^{-1}·kPa^{-1}; figure 3a) so was chosen as the final model. The most significant predictor of K was RBC:gas, whereas sex was the highest-ranking predictor of V_A (figure 3b). This is expected because sex is strongly correlated with height, which in turn is a significant predictor of lung volume [37]. The model also performed well when applied to the validation data (figure 3c; MAE=0.840 mmol·min^{-1}·kPa^{-1},
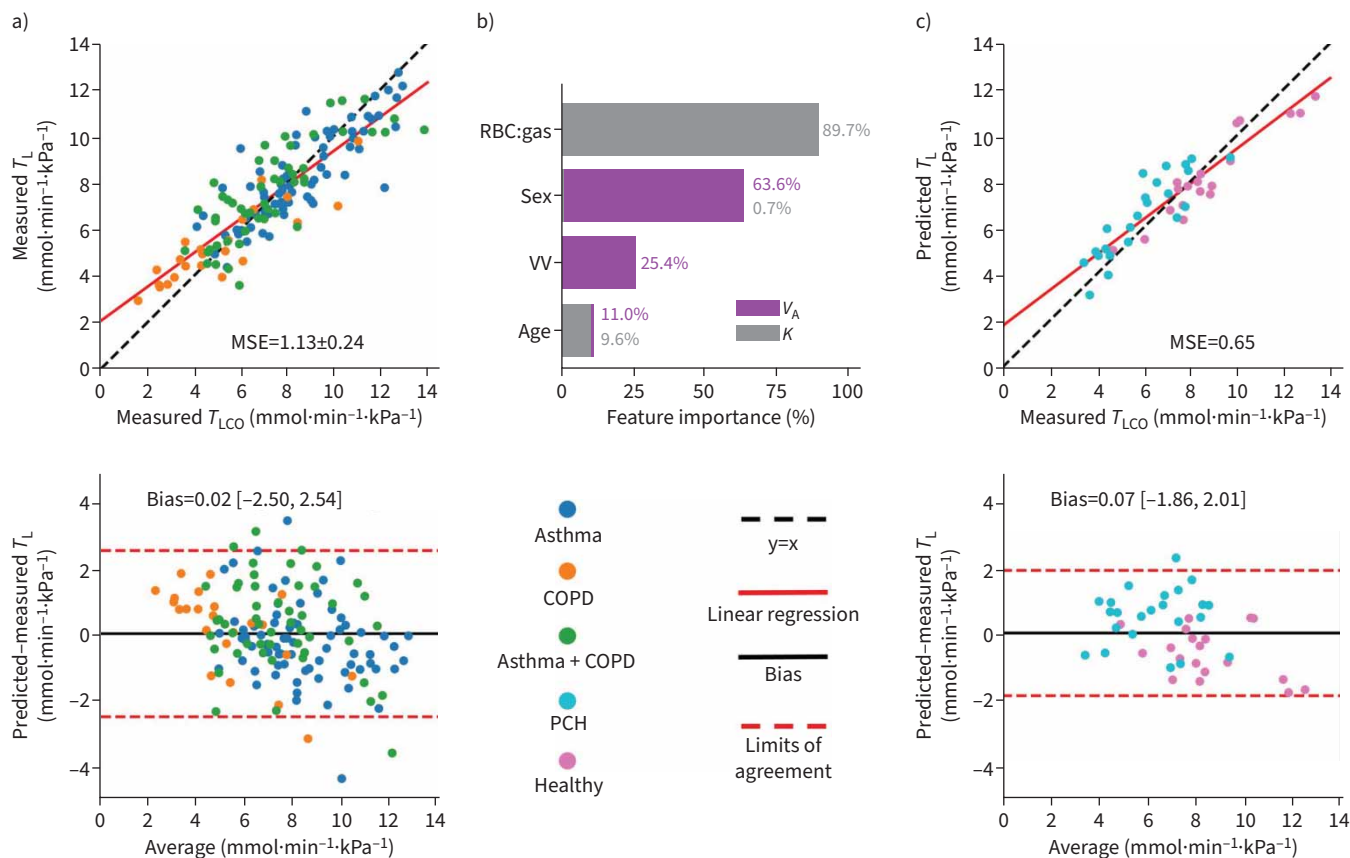
FIGURE 3 Random forest regression model. a) Linear regression (top) and Bland–Altman (bottom) plots of the measured and random forest-predicted transfer factor values for the training data. b) ranked importance of the prediction variables. c) Linear regression (top) and Bland–Altman (bottom) plots for the measured and random forest-predicted transfer factor values for the validation group. T_L: transfer factor of the lungs; MSE: mean squared error; T_{LCO}: T_L for carbon monoxide; RBC: red blood cells; V_A: alveolar ventilation; V: ventilated volume; PCH: post-COVID-19 hospitalisation; K: transfer coefficient.

MSE=0.647·mmol^2·min^{-2}·kPa^{-2}, R^2=0.828). For completeness, models 1a, 1b and 2 were also evaluated on the validation data (supplementary figure 1) and the performance of model 2 was found to be slightly better that of model 3: MAE=0.744 mmol·min^{-1}·kPa^{-1}, MSE=0.452·mmol^2·min^{-2}·kPa^{-2}, R^2=0.877.
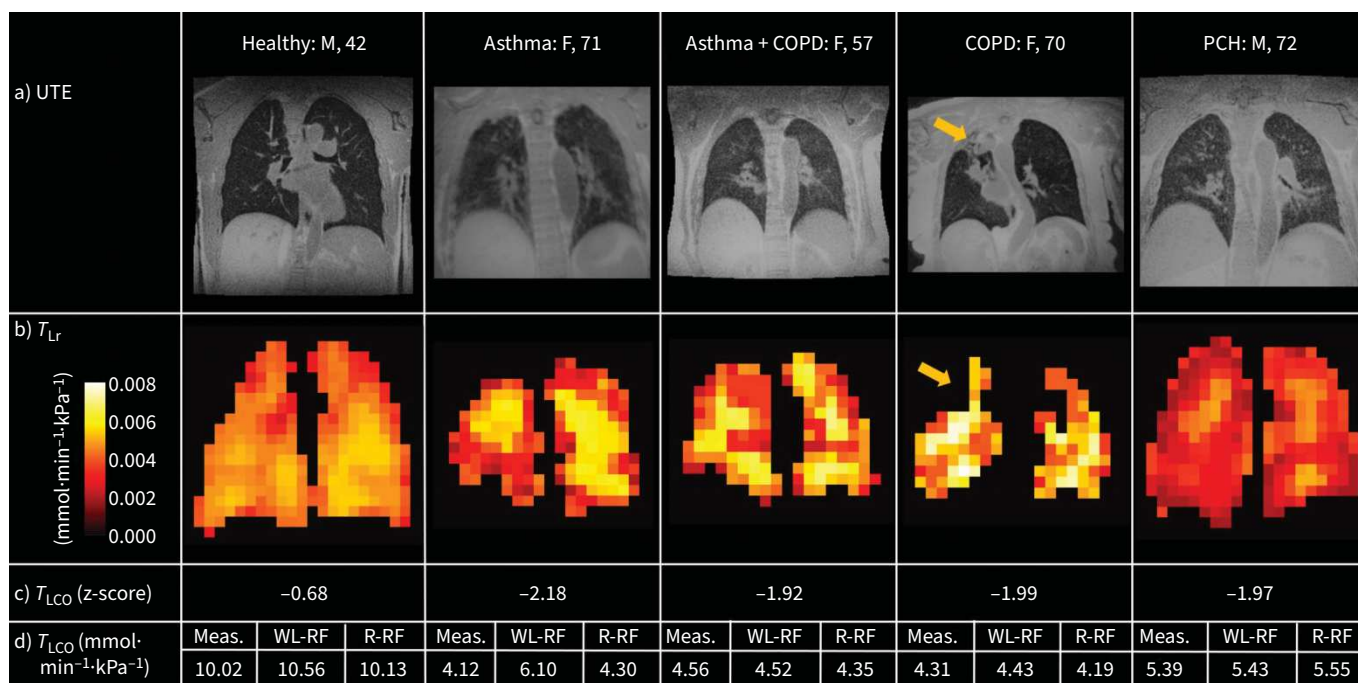
Regional T_{LCO} prediction

Example predicted T_L maps demonstrating differences between four participants with different pathology, but similar T_{LCO} z-scores, and one healthy volunteer are shown in figure 4. With the addition of regional gas exchange information, the performance of the random forest model was not improved when compared with the whole-lung model, but was still reasonably good: MAE=1.18 mmol·min^{-1}·kPa^{-1}, MSE=1.26·mmol^2·min^{-2}·kPa^{-2}, R^2=0.736. It also performed well when applied to visit two data from the same study, for both pre-bronchodilator (MAE=1.30 mmol·min^{-1}·kPa^{-1}, MSE=1.17 mmol^2·min^{-2}·kPa^{-2}, R^2=0.747) and post-bronchodilator (MAE=1.14 mmol·min^{-1}·kPa^{-1}, MSE=1.13 mmol^2·min^{-2}·kPa^{-2}, R^2=0.756) data. Linear regression and Bland–Altman plots comparing the measured, whole-lung random forest-predicted and regional random forest-predicted T_L values for both visits are shown in supplementary figure 2. Example T_L-constituent K_{CO} and V_A maps for one participant with both asthma and COPD are shown in figure 5. This person had normal measured T_{LCO} (z-score=0.48), but their maps reveal regional heterogeneity in both ventilation and gas transfer.
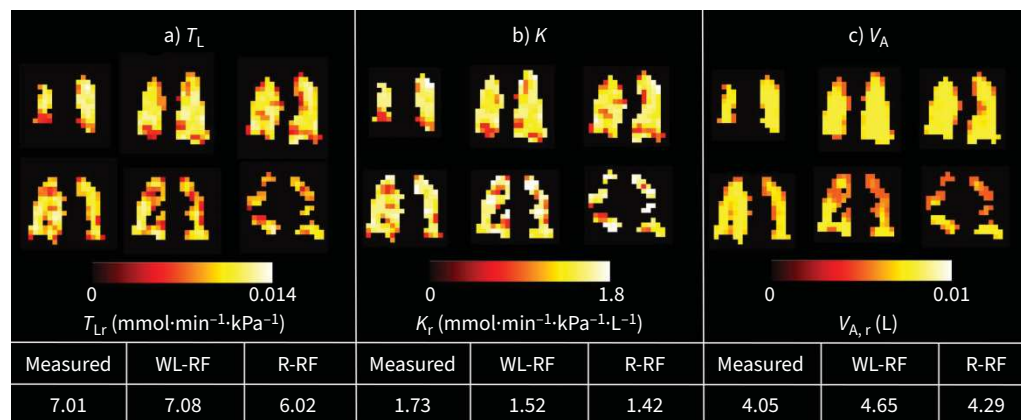
Figure 6 shows the predicted T_L, K and V_A maps for a single slice for a participant with both asthma and COPD before and after bronchodilator administration. The maps show an increase in the lung mask area post-bronchodilator, but the gas signal intensity per voxel decreases because the same amount of gas is distributed over more voxels due to the opening of previously unventilated airways. Changes in the regional distribution of T_L, K and V_A following bronchodilator can be assessed by considering the predicted values for each lung slice (figure 6, bottom panel).

Discussion

In this work, we have demonstrated that random forest regression improves prediction of T_L from ^{129}Xe MRI metrics when compared with a physiology-based model. We then go on to apply this model to create maps of T_L, K and V_A. This approach provides a valuable means to visualise these clinical lung physiology

	Healthy: M, 42	Asthma: F, 71	Asthma + COPD: F, 57	COPD: F, 70	PCH: M, 72
a) UTE					

b) T_{Lr} (mmol·min^{-1}·kPa^{-1})

0.008
0.006
0.004
0.002
0.000

c) T_{LCO} (z-score)	−0.68			−2.18			−1.92			−1.99			−1.97		
d) T_{LCO} (mmol·min^{-1}·kPa^{-1})	Meas.	WL-RF	R-RF	Meas.	WL-RF	R-RF	Meas.	WL-RF	R-RF	Meas.	WL-RF	R-RF	Meas.	WL-RF	R-RF
	10.02	10.56	10.13	4.12	6.10	4.30	4.56	4.52	4.35	4.31	4.43	4.19	5.39	5.43	5.55

FIGURE 4 a) Ultrashort echo time (UTE) lung structure images and b) random forest regression-predicted transfer factor of the lung (T_L) maps for five participants and their diagnosis, sex and age, and c) T_L for carbon monoxide (T_{LCO}) z-score at visit one. The fourth patient shown in a) had a lack of xenon-129 signal in the upper right lung due to underlying structural changes (yellow arrows). d) The measured and estimated T_L values for each participant are given, where "WL-RF" refers to the value from the whole-lung random forest model and "R-RF" refers to the value from the sum of T_{Lr} from the regional random forest model over all voxels. M: male; F: female; PCH: post-COVID-19 hospitalisation.
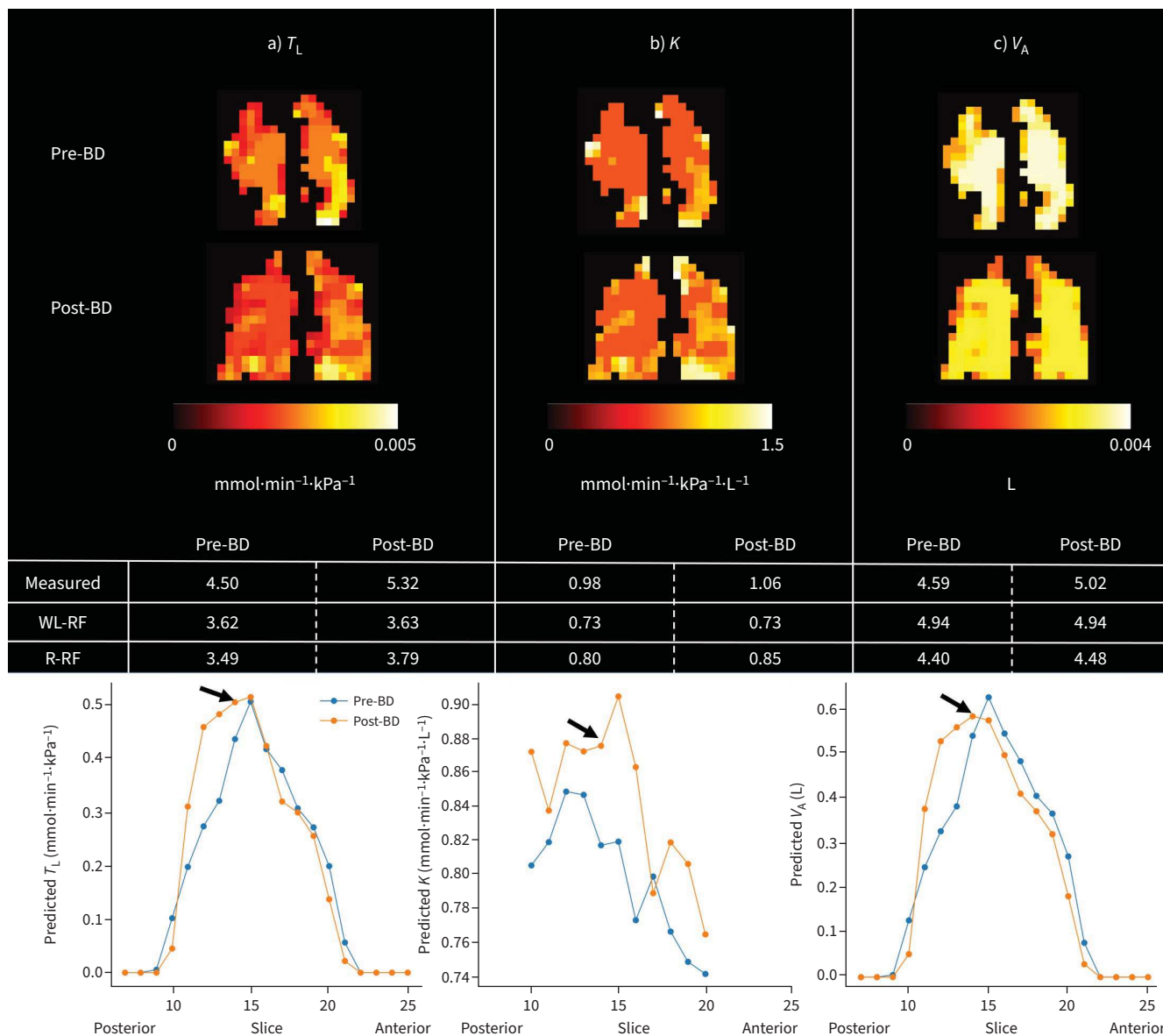
	a) T_L			b) K			c) V_A	
	T_{Lr} (mmol·min^{-1}·kPa^{-1})			K_r (mmol·min^{-1}·kPa^{-1}·L^{-1})			$V_{A,r}$ (L)	
Measured	WL-RF	R-RF	Measured	WL-RF	R-RF	Measured	WL-RF	R-RF
7.01	7.08	6.02	1.73	1.52	1.42	4.05	4.65	4.29

FIGURE 5 Random forest regression modelled a) transfer factor of the lung (T_L), b) transfer coefficient (K) and c) alveolar volume (V_A) maps for a 57-year-old female patient with both asthma and COPD for six lung slices, plus the modelled and measured whole-lung values at visit one. "WL-RF" refers to the value from the whole-lung random forest model and "R-RF" refers to the value from the regional random forest model. Although this patient had a normal T_L for carbon monoxide (T_{LCO}) (as measured by pulmonary function testing), their T_L map indicates reduced gas exchange. The K map shows a heterogeneous gas transfer rate which does not match the ventilation distribution.

metrics at a regional level, allowing the contributions from the ventilation distribution and gas uptake rate to be examined, and links measures from ^{129}Xe gas exchange imaging to well-established physiological quantities.

Three models for predicting T_L from ^{129}Xe MRI data were evaluated. The coefficients from the previously proposed model [18] did not fit our data well, likely due to differences in MRI acquisition strategies/ parameters and participant disease aetiologies; the previous model was trained on data from healthy participants and those with obstructive, restrictive and pulmonary–vascular lung disease. It is also possible that, by not using cross-validation, the coefficients in [18] were reached by finding a suboptimal local minimum of MSE. In contrast to [18], we found $k_M > k_R$, which suggests a greater contribution to the total impedance from the membrane than the capillary blood, or ventilation–perfusion mismatch.

The addition of participant age and sex in the multivariable linear and random forest regression models further improved prediction accuracy when compared with the physiology-based model. Age appeared in both the K and V_A prediction, suggesting that T_{LCO} has a second-order age dependence. An age^2 dependence represents an accelerated loss of lung function with age and is also found in the T_{LCO} prediction equations of MUNKHOLM et al. [22]. All models had small SD across the five cross-validation folds, demonstrating good accuracy and minimal overfitting, but the best-performing model for the training data was random forest regression. This may be because the model is able to account for nonlinear relationships [36]; whereas equations 3 and 12 assume a linear relationship between VV (acquired at functional residual capacity +1 L) and V_A (acquired at TLC), the lung volume dependent pathophysiology in obstructive lung disease means that the relationship is likely to be more complicated.

Beyond improved modelling, a further novel aspect of this work is the application of the random forest prediction model to produce spatially localised T_L, K and V_A parametric maps, allowing for regional visualisation of otherwise global metrics. Combining the information from dissolved-phase and ventilation ^{129}Xe MRI, along with patient age and sex, into a parametric map with defined units may provide a way for respiratory physicians to easily interpret ^{129}Xe gas exchange MRI. T_L mapping could assist in the phenotyping of patients and in assessing longitudinal changes and treatment response, especially for patients with both gas exchange limitation and ventilation heterogeneity. One of the key assumptions in the T_{LCO} PFT is that the inspired test gas is homogeneously distributed throughout the lung. However, in obstructive lung disease, ventilation is heterogeneous and so this assumption may not be appropriate and can lead to an underestimation of T_{LCO} [38]. Contrarily, our models use regional gas exchange measurements from dissolved ^{129}Xe MRI to estimate transfer factor of the lung T_L, which are intrinsically sensitive to the distribution of ^{129}Xe gas in the lungs. This may explain why the models consistently overestimated T_L for COPD patients with low measured T_{LCO} values.

	Pre-BD	Post-BD	Pre-BD	Post-BD	Pre-BD	Post-BD
Measured	4.50	5.32	0.98	1.06	4.59	5.02
WL-RF	3.62	3.63	0.73	0.73	4.94	4.94
R-RF	3.49	3.79	0.80	0.85	4.40	4.48

FIGURE 6 Predicted maps of a) transfer factor of the lung (T_L), b) transfer coefficient (K) and c) alveolar volume (V_A) for a single lung slice for a 61-year-old female with both asthma and COPD pre- and post-bronchodilator (BD). The sum (mean for K_r) for each slice (posterior to anterior) is plotted, showing the change in distribution following BD administration. The lung slice is indicated with an arrow. These plots show that $V_{A,r}$ and T_{Lr} increase in the posterior lung following BD, while slightly decreasing in the central and anterior slices.

T_L was often underestimated for participants with high measured T_{LCO}. This may be due to the larger error on predicted T_L (δT_L) for higher T_{LCO} values. T_L was found from the product of the predicted V_A and K values/maps and so the error on these components is propagated through to T_L according to error propagation formula:

$$\delta T_L = T_L \sqrt{\left(\frac{\delta V_A}{V_A}\right)^2 + \left(\frac{\delta K}{K}\right)^2} \qquad (13)$$

Inherent differences between ^{129}Xe MRI and T_{LCO} measurement, such as the diffusivity and solubility of the gases used and the lung volumes and body positions, may also limit the predictive power of the models. Although the random forest and linear regression models improved the prediction of T_L, with these models the ability to estimate the membrane and capillary blood conductance is lost. Another limitation of

our work is the requirement for both ventilation and gas exchange ^{129}Xe imaging, which necessitates two separate acquisitions with up to 1.5 L of xenon. At present it is not practical to calculate VV from the gas exchange imaging gas-phase image, because the image resolution (1.25 cm^3 voxel size) is too low for reliable registration with the anatomical proton image. However, image acceleration techniques such as compressed sensing and rapid spiral k-space encoding gradients may make a combined ventilation and gas exchange imaging sequence feasible [39].

The models in this work were trained solely on patients with obstructive lung disease and their application to patients with restrictive and pulmonary–vascular disease and patients from a different site has not been explored. There are still considerable differences between the ^{129}Xe MRI sequences and acquisition parameters used between sites, which may limit the application of our models to external data; however, efforts towards harmonisation are being made through the ^{129}Xe MRI Clinical Trials Consortium [40]. Hence, it is possible that some retraining could be required to tune the model parameters for external data, but we anticipate that the models themselves and the principle of using regression modelling to map T_L should be generalisable. We have attempted to reduce overfitting by using a five-fold cross-validation training strategy and used training data from a heterogeneous population with a large range of T_{LCO} values (1.60–13.86 mmol·min^{-1}·kPa^{-1}). The models performed well on validation data from two different clinical studies, with different patient groups and acquisition parameters to the training data, suggesting generalisability to other lung diseases. This is despite the bias between the datasets from differences in repetition time and flip angle in the dissolved ^{129}Xe imaging sequence. Testing the models on different patient cohorts and on external data is required to fully assess their generalisability.

In conclusion, regional T_{LCO} can be modelled from ^{129}Xe MRI metrics for patients with obstructive lung disease. Prediction accuracy was greatest with a random forest regression model which used patient age, sex and ^{129}Xe MRI-derived VV and RBC:gas as prediction variables. The ability of this model to generate T_L maps presents a useful tool for visualisation and interpretation of regional T_L limitation and should help facilitate the clinical translation of ^{129}Xe gas exchange MRI.

References

1   Modi P, Cascella M. Diffusing Capacity of the Lungs for Carbon Monoxide. Treasure Island (FL), StatPearls Publishing, 2023.

2   Heckman EJ, O'Connor GT. Pulmonary function tests for diagnosing lung disease. *JAMA* 2015; 313: 2278–2279.

3   Virgincar RS, Cleveland ZI, Sivaram Kaushik S, *et al.* Quantitative analysis of hyperpolarized 129Xe ventilation imaging in healthy volunteers and subjects with chronic obstructive pulmonary disease. *NMR Biomed* 2013; 26: 424–435.

4   He M, Driehuys B, Que LG, *et al.* Using hyperpolarized 129Xe MRI to quantify the pulmonary ventilation distribution. *Acad Radiol* 2016; 23: 1521–1531.

5   Kaushik SS, Robertson SH, Freeman MS, *et al.* Single-breath clinical imaging of hyperpolarized Xe-129 in the airspaces, barrier, and red blood cells using an interleaved 3D radial 1-point Dixon acquisition. *Magn Reson Med* 2016; 75: 1434–1443.

6   Cleveland ZI, Virgincar RS, Qi Y, *et al.* 3D MRI of impaired hyperpolarized Xe-129 uptake in a rat model of pulmonary fibrosis. *NMR Biomed* 2014; 27: 1502–1514.

7   Collier GJ, Eaden JA, Hughes PJC, *et al.* Dissolved Xe-129 lung MRI with four-echo 3D radial spectroscopic imaging: quantification of regional gas transfer in idiopathic pulmonary fibrosis. *Magn Reson Med* 2021; 85: 2622–2633.

8   Qing K, Ruppert K, Jiang Y, *et al.* Regional mapping of gas uptake by blood and tissue in the human lung using hyperpolarized xenon-129 MRI. *J Magn Reson Imaging* 2014; 39: 346–359.

9   Kammerman J, Hahn AD, Cadman RV, *et al.* Transverse relaxation rates of pulmonary dissolved-phase hyperpolarized Xe-129 as a biomarker of lung injury in idiopathic pulmonary fibrosis. *Magn Reson Med* 2020; 84: 1857–1867.

10   Qing K, Mugler JP, Altes TA, *et al.* Assessment of lung function in asthma and COPD using hyperpolarized Xe-129 chemical shift saturation recovery spectroscopy and dissolved-phase MRI. *NMR Biomed* 2014; 27: 1490–1501.

11   Wang ZY, Bier EA, Swaminathan A, *et al.* Diverse cardiopulmonary diseases are associated with distinct xenon magnetic resonance imaging signatures. *Eur Respir J* 2019; 54: 1900831.

12   Ruppert K, Altes TA, Mata JF, *et al.* Detecting pulmonary capillary blood pulsations using hyperpolarized xenon-129 chemical shift saturation recovery (CSSR) MR spectroscopy. *Magn Reson Med* 2016; 75: 1771–1780.

13   Mummy DG, Bier EA, Wang ZY, *et al.* Hyperpolarized Xe-129 MRI and spectroscopy of gas-exchange abnormalities in nonspecific interstitial pneumonia. *Radiology* 2021; 301: 211–220.

14   Wang JM, Robertson SH, Wang ZY, *et al.* Using hyperpolarized Xe-129 MRI to quantify regional gas transfer in idiopathic pulmonary fibrosis. *Thorax* 2018; 73: 21–28.

15   Grist JT, Chen M, Collier GJ, *et al.* Hyperpolarized Xe-129 MRI abnormalities in dyspneic patients 3 months after COVID-19 pneumonia: preliminary results. *Radiology* 2021; 301: E353–E360.

16   Grist JT, Collier GJ, Walters H, *et al.* Lung abnormalities detected with hyperpolarized [129]Xe MRI in patients with long COVID. *Radiology* 2022; 305: 709–717.

17   Saunders LC, Collier GJ, Chan H-F, *et al.* Longitudinal lung function assessment of patients hospitalized with COVID-19 using ^{1}H and [129]Xe lung MRI. *Chest* 2023; 164: 700–716.

18   Wang ZY, Rankine L, Bier EA, *et al.* Using hyperpolarized Xe-129 gas-exchange MRI to model the regional airspace, membrane, and capillary contributions to diffusing capacity. *J Appl Physiol (1985)* 2021; 130: 1398–1409.

19   Aguilaniu B, Maitre J, Glénet S, *et al.* European reference equations for CO and NO lung transfer. *Eur Respir J* 2008; 31: 1091–1097.

20   Quanjer PH, Stanojevic S, Cole TJ, *et al.* Multi-ethnic reference values for spirometry for the 3–95-yr age range: the global lung function 2012 equations. *Eur Respir J* 2012; 40: 1324–1343.

21   Stanojevic S, Graham BL, Cooper BG, *et al.* Official ERS technical standards: Global Lung Function Initiative reference values for the carbon monoxide transfer factor for Caucasians. *Eur Respir J* 2017; 50: 1700010.

22   Munkholm M, Marott JL, Bjerre-Kristensen L, *et al.* Reference equations for pulmonary diffusing capacity of carbon monoxide and nitric oxide in adult Caucasians. *Eur Respir J* 2018; 52: 1500677.

23   Plummer JW, Willmering MM, Cleveland ZI, *et al.* Childhood to adulthood: accounting for age dependence in healthy-reference distributions in [129]Xe gas-exchange MRI. *Magn Reson Med* 2023; 89: 1117–1133.

24   Collier GJ, Smith LJ, Saunders LC, *et al.* Age, sex, and lung volume dependence of dissolved xenon-129 MRI gas exchange metrics. *Magn Reson Med* 2024; 92: 1471–1483.

25   Mummy D, Zhang S, Bechtel A, *et al.* Functional gas exchange measures on (129)Xe MRI and spectroscopy are associated with age, sex, and BMI in healthy subjects. *Front Med* 2024; 11; 1342499.

26   West JB. Respiratory Physiology. Baltimore, Lippencott Williams and Wilkins, 2008.

27   Woodhouse N, Wild JM, Paley MNJ, *et al.* Combined helium-3/proton magnetic resonance imaging measurement of ventilated lung volumes in smokers compared to never-smokers. *J Magn Reson Imaging* 2005; 21: 365–369.

28   Reddel HK, Gerhardsson de Verdier M, Agustí A, *et al.* Prospective observational study in patients with obstructive lung disease: NOVELTY design. *ERJ Open Res* 2019; 5: 00036-2018.

29   Marshall H, Wild JM, Smith LJ, *et al.* Functional imaging in asthma and COPD: design of the NOVELTY ADPro substudy. *ERJ Open Res* 2023; 9: 00344-2022.

30 Ng K, Saunders LC, Collier G, *et al.* The EXPLAIN (Hyperpolarised Xenon Magnetic Resonance Pulmonary Imaging in Patients with Long-COVID) Study: the primary outcome. *Am J Respir Crit Care Med* 2024; 209: A6478.

31 Norquay G, Collier GJ, Rao M, *et al.* 129Xe-Rb spin-exchange optical pumping with high photon efficiency. *Phys Rev Lett* 2018; 121: 153201.

32 Stewart NJ, Norquay G, Griffiths PD, *et al.* Feasibility of human lung ventilation imaging using highly polarized naturally abundant xenon and optimized three-dimensional steady-state free precession. *Magn Reson Med* 2015; 74: 346–352.

33 Johnson KM, Fain SB, Schiebler ML, *et al.* Optimized 3D ultrashort echo time pulmonary MRI. *Magn Reson Med* 2013; 70: 1241–1250.

34 Graham BL, Brusasco V, Burgos F, *et al.* 2017 ERS/ATS standards for single-breath carbon monoxide uptake in the lung. *Eur Respir J* 2017; 49: 1600016.

35 Pedregosa F, Varoquaux G, Gramfort A, *et al.* Scikit-learn: machine learning in Python. *J Mach Learn Res* 2011; 12: 2825–2830.

36 Breiman L, Random forests. *Machine Learn* 2001; 45: 5–32.

37 Cook CD, Hamann JF. Relation of lung volumes to height in healthy persons between the ages of 5 and 38 years. *J Pediatr* 1961; 59: 710–714.

38 Hughes M. Physiology and Practice of Pulmonary Function. London, Association for Respiratory Technology and Physiology, 2009.

39 Niedbalski PJ, Willmering MM, Thomen RP, *et al.* A single-breath-hold protocol for hyperpolarized [129]Xe ventilation and gas exchange imaging. *NMR Biomed* 2023; 36: e4923.

40 Niedbalski PJ, Hall CS, Castro M, *et al.* Protocols for multi-site trials using hyperpolarized 129 Xe MRI for imaging of ventilation, alveolar-airspace size, and gas exchange: a position paper from the 129 Xe MRI clinical trials consortium. *Magn Reson Med* 2021; 86: 2966–2986.